The VIMOS VLT deep survey. Computing the two point correlation statistics and associated uncertainties

Agnieszka Pollo, Baptiste Meneux, L. Guzzo, Olivier Le Fèvre, J. Blaizot, A. Cappi, Angela Iovino, Christian Marinoni, Henry J. Mccracken, D. Bottini, et al.

A&A 439, 887–900 (2005)
DOI: 10.1051/0004-6361:20041964

Astronomy & Astrophysics

The VIMOS VLT deep survey⋆

Computing the two point correlation statistics and associated uncertainties

A. Pollo[1], B. Meneux[2], L. Guzzo[1], O. Le Fèvre[2], J. Blaizot[2], A. Cappi[3], A. Iovino[4], C. Marinoni[2], H. J. McCracken[5,6] D. Bottini[7], B. Garilli[7], V. Le Brun[2], D. Maccagni[7], J. P. Picat[8], R. Scaramella[9], M. Scodeggio[7], L. Tresse[2], G. Vettolani[10], A. Zanichelli[10], C. Adami[2], M. Arnaboldi[13], S. Arnouts[2], S. Bardelli[3], M. Bolzonella[3], S. Charlot[5,11], P. Ciliegi[10], T. Contini[8], S. Foucaud[7], P. Franzetti[7], I. Gavignaud[8], O. Ilbert[2], B. Marano[12], G. Mathez[8], A. Mazure[2], R. Merighi[3], S. Paltani[2], R. Pellò[8], L. Pozzetti[3], M. Radovich[13], G. Zamorani[3], E. Zucca[3], M. Bondi[10], A. Bongiorno[3], G. Busarello[13], L. Gregorini[10], F. Lamareille[8], Y. Mellier[5,6], P. Merluzzi[13], V. Ripepi[13], and D. Rizzo[8]

[1] INAF – Osservatorio Astronomico di Brera, via Bianchi 46, Merate (LC), Italy
e-mail: apollo@merate.mi.astro.it
[2] Laboratoire d'Astrophysique de Marseille, UMR 6110 CNRS, Université de Provence, Traverse du Siphon-Les trois Lucs, 13012 Marseille, France
[3] INAF – Osservatorio Astronomico di Bologna, via Ranzani 1, 40127 Bologna, Italy
[4] INAF – Osservatorio Astronomico di Brera, via Brera, 20121 Milan, Italy
[5] Institut d'Astrophysique de Paris, UMR 7095, 98bis Bd. Arago, 75014 Paris, France
[6] Observatoire de Paris, LERMA, UMR 8112, 61 Av. de l'Observatoire, 75014 Paris, France
[7] IASF – INAF, 20133 Milano, Italy
[8] Laboratoire d'Astrophysique – Observatoire Midi-Pyrénées, 31400 Toulouse, France
[9] INAF – Osservatorio Astronomico di Roma, Italy
[10] INAF – Istituto di Radio-Astronomia, Bologna, Italy
[11] Max-Planck-Institut für Astrophysik, 85741 Garching, Germany
[12] Università di Bologna, Departimento di Astronomia, via Ranzani 1, 40127 Bologna, Italy
[13] INAF – Osservatorio Astronomico di Capodimonte, via Moiariello 16, 80131 Napoli, Italy

Received 6 September 2004 / Accepted 10 March 2005

Abstract. We present a detailed description of the methods used to compute the three-dimensional two-point galaxy correlation function in the VIMOS-VLT deep survey (VVDS). We investigate how instrumental selection effects and observational biases affect the measurements and identify the methods to correct for them. We quantify the accuracy of our corrections using an ensemble of 50 mock galaxy surveys generated with the *GalICS* semi-analytic model of galaxy formation which incorporate the selection biases and tiling strategy of the real data. We demonstrate that we are able to recover the real-space two-point correlation function $\xi(s)$ and the projected correlation function $w_{\rm p}(r_{\rm p})$ to an accuracy better than 10% on scales larger than 1 h^{-1} Mpc with the sampling strategy used for the first epoch VVDS data. The large number of simulated surveys allows us to provide a reliable estimate of the cosmic variance on the measurements of the correlation length r_0 at $z \sim 1$, of about 15–20% for the first epoch VVDS observation while any residual systematic effect in the measurements of r_0 is always below 5%. The error estimation and measurement techniques outlined in this paper are being used in several parallel studies which investigate in detail the clustering properties of galaxies in the VVDS.

Key words. cosmology: large scale structure of Universe – methods: statistical – galaxies: evolution – surveys

1. Introduction

The VIMOS VLT Deep Survey (VVDS, Le Fèvre et al. 2005a) is dedicated to study the evolution of galaxies and large scale structure to $z \sim 2$ with a significant fraction of galaxies reaching $z \sim 4$. The VVDS spectroscopic survey is performed with the VIMOS spectrograph at the European Southern Observatory Very Large Telescope and complemented with multi-color BVRI imaging data obtained at the CFHT telescope (McCracken et al. 2003; Le Fèvre et al. 2004). The complete survey will consist of four fields of 2° by 2° each, with multi-band photometry coverage in the *BVRI* (and partly *UJK*) bands.

⋆ Based on data obtained with the European Southern Observatory Very Large Telescope, Paranal, Chile, program 070.A-9007(A), and on data obtained at the Canada-France-Hawaii Telescope, operated by the CNRS of France, CNRC in Canada and the University of Hawaii.

Multi-object spectroscopy down to $I_{AB} = 22.5$ is being obtained over the four fields ("VVDS Wide"), with a deeper area of 1.5 deg^2 in the VVDS-02h and in the Chandra Deep Field South (VVDS-CDFS) covered to $I_{AB} = 24$ ("VVDS Deep"). The first epoch VVDS data consist of more than 11 000 spectra obtained in the VVDS-Deep fields (Le Fèvre et al. 2005a).

One of the key science goals of the VVDS is to measure the evolution of galaxy clustering from the present epoch up to $z \sim 2$. The simplest statistic used for this analysis is the spatial two-point correlation function $\xi(r)$ and its variants, (e.g. Peebles 1980), i.e. the second moment of the galaxy distribution. Given the geometry and selection function of galaxy surveys, however, the practical estimation of $\xi(r)$ from the actual data is not straightforward. Edge effects, sampling inhomogeneities and selection effects all introduce different biases that hamper the survey's ability to estimate the true underlying clustering process. Moreover, intrinsic systematic uncertainties due to the limited size of the volume of the Universe explored ("cosmic variance") need to be accounted for when computing realistic error bars on the measured correlation values.

The aim of this paper is to present a comprehensive description of the biases specific to the VVDS, along with the methods we developed to correct for them. The strategy we adopt relies on the construction of realistic "pre-observation" mock catalogs using the *MoMaF* software (Blaizot et al. 2005) and the *GalICS* hybrid model for galaxy formation (Hatton et al. 2003). We then observe these mock catalogs, by mimicking the relevant observational selections and biases. Comparing original and observed mock surveys allows us to (i) quantitatively understand the impact of the different biases inherent to the VVDS data on clustering estimates, and (ii) to explore and validate methods that allow us to recover the original signal. This strategy is possible because *GalICS* predictions have been shown to agree fairly well with a wide range of observations (e.g. Hatton et al. 2003; Blaizot et al. 2004), and is thus expected to yield catalogs realistic enough to carry out a convincing consistency check. Because our mock catalogs contain realistic clustering properties, we can also use them to predict the cosmic variance amplitude in order to compute realistic errors on the clustering estimates we will perform on the real data.

The paper is organized as follows. In Sect. 2 we discuss the different kind of biases expected in the current VVDS first-epoch data. In Sect. 3 we discuss the construction of mock VVDS catalogs from the *GalICS*/*MoMaf* simulations which assume a flat Cold Dark Matter model with $\Omega_{\rm m} = 0.333$, $\Omega_\Lambda = 0.667$ and $h = 0.667$. In Sect. 4 we present the definitions of the two-point correlation functions. Then, in Sect. 5 we discuss the details of the error measurement strategy when applied to VVDS. In Sect. 6 we show how the measured two-point correlation function is affected by the features particular to our survey and we discuss the methods developed to correct for these biases and properly estimate the correlation function $\xi(r_{\rm p}, \pi)$, its projection $w_{\rm p}(r_{\rm p})$, and the correlation length r_0 and slope γ, as a function of redshift. Section 7 summarizes our results.

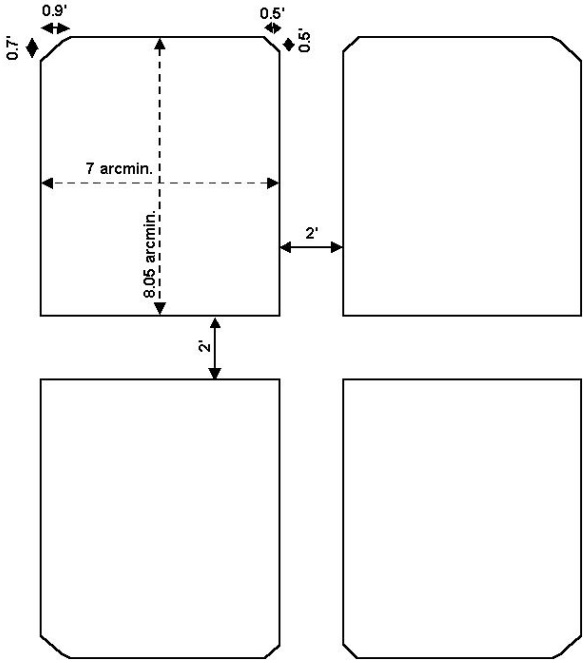

Fig. 1. Lay-out of the VIMOS field of view. INVAR masks with laser-cut slits are placed on the focal plane within the four rectangular areas ("VIMOS channels").

2. The selection function of VVDS first epoch observations

The first epoch spectra of the VVDS-Deep collected during the 2002 and 2003 campaigns are concentrated within the 02h deep field, and the CDFS (Le Fèvre et al. 2005a). First epoch spectra have been collected for galaxies down to $I_{AB} \leq 24$ in the 0.61 sq degree sub-area of the VVDS-02h field and a region of 21×21.6 sq arcmin centered on the Chandra Deep Field South (CDFS, Giacconi et al. 2002). The VVDS First Epoch data geometrical lay-out, sampling rate and incompleteness are used as a reference benchmark in this paper.

2.1. Catalog structure and biases

A number of factors, both in the parent photometric catalog from which the target galaxies are selected and in the way the spectroscopic observations are carried out, contribute to create selection effects that bias any estimate of galaxy clustering if not properly accounted for.

1. **Photometric defects.** Some areas are excised from the *I*-band CCD images during their photometric analysis, due to the presence of bright stars or other instrumental effects (e.g. stray-light from a bright star outside the field of view). The resulting photometric galaxy catalog, therefore, features some artificially empty regions.
2. **VIMOS lay-out.** The field of view of the VIMOS spectrograph consists of four 7′ by 8′ quadrants, separated by 2′ gaps, as shown schematically in Fig. 1. At the typical resolution used in the VVDS, between 110 and 150 spectra are collected in each quadrant during a single observation. Clearly, no galaxies are observed over the area

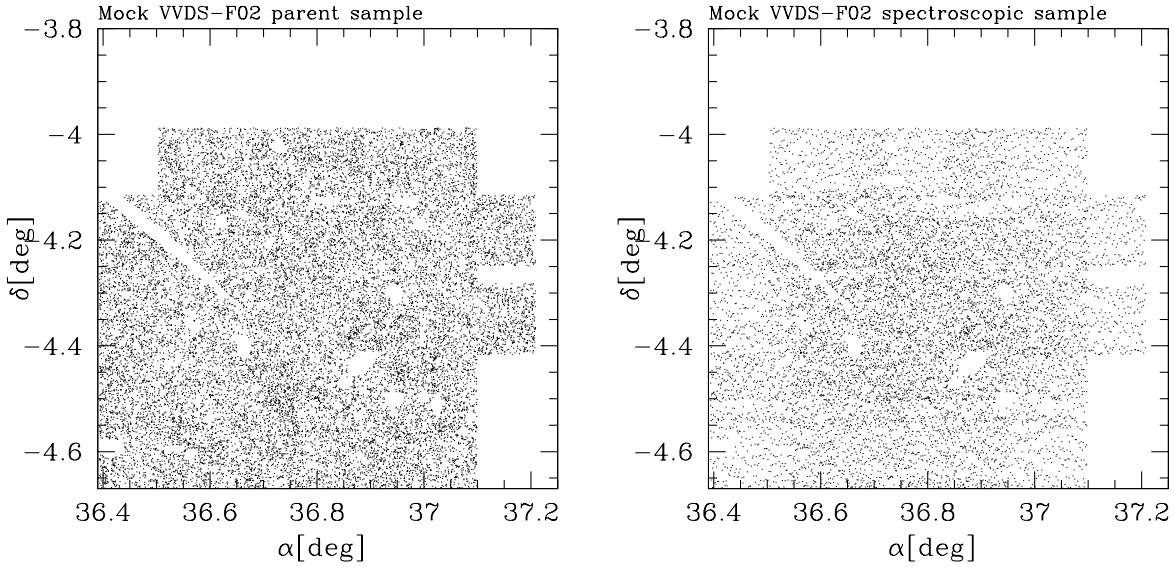

Fig. 2. Galaxy distribution in a mock VVDS-02h catalog, constructed using the *GalICS* simulations with the same lay-out as the 20 observed pointings in the actual first-epoch VVDS field and applying the full range of selection effects present in the data, as e.g. the photometric mask. The left panel shows the parent photometric field, including all objects with $I_{AB} \leq 24$ within the current VVDS-02h boundaries and mask. In the right panel only the objects selected for spectroscopy are shown. Note the density gradient towards the central part of the field, due to multiple passes over the same area.

of the "cross" between the four quadrants, unless one observes the area with a new pointing, shifted with respect to the first one (see below).

3. **Missing quadrants.** For a few pointings, one or two quadrants can be "blind", i.e. with no spectra observed due to a misplacement of the multi-slit masks during the observations.
4. **Incomplete coverage.** The planned final area is being covered through a mosaic of adjacent pointings. Thus, at any intermediate stage the available spectral data set is distributed in a non-uniform fashion on the sky. The largest contiguous area currently covered in the 02h deep field corresponds to about 0.5 square degrees, with the geometry shown in Fig. 2.
5. **Varying sampling density.** The VVDS observational strategy involves multiple passes over the same area to increase the spectral sampling rate. While a central region of the 02h deep field is exposed 4 times (i.e. it is visited by four independent pointings with different slit masks), the external areas are covered only twice due to the tiling strategy. During subsequent observing runs, the VIMOS pointings are shifted with respect to the previous ones usually by around 2′, to ensure that the cross visible in Fig. 1 is filled. As a consequence, the mean surface density of observed objects varies across the field.
6. **Optimization of the number of slits and mechanical constraints.** A specific source of bias in the VIMOS observations is introduced by VMMPS – the VIMOS Mask Manufacturing Preparation Software, and specifically by the Super-SPOC code (Bottini et al. 2005). The width of a slit is set to 1 arcsec (or about 5 detector pixels), and its typical length is ∼6−10 arcsec to include both the object of interest and enough information on the sky spectral background to correct for it. The VMMPS software automatically allocates slits to objects in the input catalog with the goal of maximizing the total number of spectra. In general, this means that the spectroscopic sample is not a random sparse sampling of the clustering pattern over the sky, but a more homogeneous sub-sample. Specifically, VMMPS tends to place objects in rows, so to maximize the number of spectra across the CCD (see Fig. 3), with an additional slight preference towards objects of small angular size. As typical with multi-object spectrographs, the minimum slit size implies that, after one single spectroscopic pass, there is a bias against observing very close angular pairs on the sky. Having multiple passes, however, significantly improves the situation, allowing for very close pairs to be observed in subsequent exposures.

The final spectroscopic sample is thus affected to different degrees by all these factors. Figure 2 shows the current lay-out of the observed pointings in the 02h field, compared to the parent photometric sample over the same area. Features from the two main effects are obvious from Fig. 2: holes in the parent catalog and the varying sampling density in the spectroscopic data, due to the multiple passes over the central area. The "striping" effect due to the slit-placing software is not obvious at this resolution and is better appreciated in Fig. 3, where only one quadrant is displayed.

3. Constructing mock VVDS surveys

The only way to understand the relative importance of the selection biases discussed above and test possible correction schemes is to create and analyze realistic simulations of our survey. Provided these simulations are realistic enough, they allow us (1) to understand quantitatively the magnitude of observational biases on the final statistical quantities to be measured, and (2) to estimate realistic errors that include cosmic

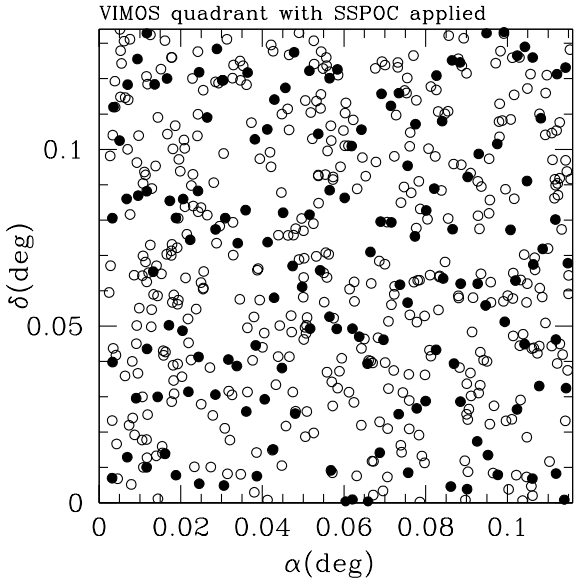

Fig. 3. Spectroscopic targets (filled circles) selected in one of the four VIMOS quadrants from a complete VVDS mock photometric sample (open circles). Note how the optimization software tends to select spectroscopic targets aligned along horizontal rows, while, clearly, very close pairs are not observed. Typically, however, 4 independent observations are conducted on the same area, each with a similar target layout, but shifted by a few arcminutes. This significantly reduces both the alignment and proximity effects. The residual bias is then further corrected by the weighting scheme discussed in Sect. 4. Overall, the four passes produce a typical sampling rate of one galaxy in four.

variance. Both these points require that mock observations contain a spatial distribution of galaxies consistent with VVDS observations – so as to measure clustering and cosmic variance – along with realistic photometric and physical properties of simulated galaxies – so as to mimic selection effects. The *GalICS* model for galaxy formation (Hatton et al. 2003) along with the *MoMaF* mock observing tool (Blaizot et al. 2005) fulfill these requirements and we thus use them to build "pre-observation" catalogs that we then "observe" by progressively adding all the VVDS observational biases and selections.

In this section, we first describe the *GalICS* simulation that we use, before discussing how we build simulated VVDS observations that account for all identified biases.

3.1. The GalICS simulations

GalICS (for *Galaxies In Cosmological Simulations*, see Hatton et al. 2003) is a model of hierarchical galaxy formation which combines high resolution cosmological simulations to describe the dark matter content of the Universe with semi-analytic prescriptions to deal with the baryonic matter.

The cosmological N-body simulation we refer to throughout this paper assumes a flat cold dark matter model with a cosmological constant ($\Omega_{\rm m} = 0.333$, $\Omega_\Lambda = 0.667$). The simulated volume is a cube of side $L_{\rm box} = 100\,h^{-1}$ Mpc, with $h = 0.667$, containing 256^3 particles of mass $8.272 \times 10^9\ M_\odot$, with a smoothing length of 29.29 kpc. The power spectrum was set in agreement with the present-day abundance of rich clusters ($\sigma_8 = 0.88$, from Eke et al. 1996), and the DM density field was evolved from $z = 35.59$ to $z = 0$, outputting 100 snapshots spaced logarithmically in the expansion factor.

GalICS builds galaxies from this simulation in two steps. First, halos of DM containing more than 20 particles are identified in each snapshot using a friend-of-friend algorithm. Their merging history trees are then computed following the constituent particles from one output to the next. Second, baryons are evolved within these halo merging history trees according to a set of semi-analytic prescriptions that aim to account for e.g. heating and cooling of the gas within halos, star formation and its feedback on the environment, stellar population evolution and metal enrichment, formation of spheroids through galaxy mergers or disc instabilities.

Three main points make *GalICS* particularly suitable for this study. First, this model yields a wide range of predictions, among which luminosities (in many bands from the UV to the sub-mm), physical properties (such as sizes of galaxies), and the positions of galaxies within the simulation snapshots. Second, these properties have been shown to be in a rather good agreement with various observations (e.g. Hatton et al. 2003; Blaizot et al. 2004). Third, mock observations are readily available from the GalICS Project's web-page[1]. These mock observations include 50 catalogs of 1×1 sq deg that contain all the information we need in this study: apparent magnitudes in the *BVRI* filters used at the CFHT, apparent sizes of the galaxies, angular coordinates in the mock sky, and redshifts.

Before using *GalICS* mock samples, it is useful to state their limitations (see however Blaizot et al. 2005, for a thorough description of these). There are mainly three shortcomings to mock catalogs made using *GalICS*. First, because of the finite mass resolution of the root simulation, faint galaxies are not well described, or even missed when they lie in unresolved haloes. This is not an issue for the present study, however, because the VVDS detection limit is brighter than *GalICS*'s resolution. Second, because mock catalogs are built from a simulation of a finite volume, they involve replications of this volume, along and perpendicular to the line of sight. These replications lead to some negative bias in the correlation functions, of at most ∼10%. This is not a concern in this paper, because we just need an approximate match with the observed data in order to perform an *internal* consistency check. *GalICS* catalogs do provide an adequate match. Third, the mock catalogs do not describe density fluctuations on scales larger than the size of the simulated volume (∼100 h^{-1} Mpc). This implies that cosmic variance estimates are likely to be under-estimated if the volume probed by a mock catalog is larger than the simulated volume. This under-estimate, however, depends on the galaxy population considered: it will be large for rare objects and small for "normal" galaxies. In other words, because cosmic variance is basically given by the integral of the correlation function over the survey, the error on the estimated cosmic variance depends on how much of this integral we miss, that is, on how strongly the studied galaxies are clustered. From Fig. 9, it can be seen that the size of the simulation is enough for this under-estimate to be small at the scales

[1] http://galics.iap.fr

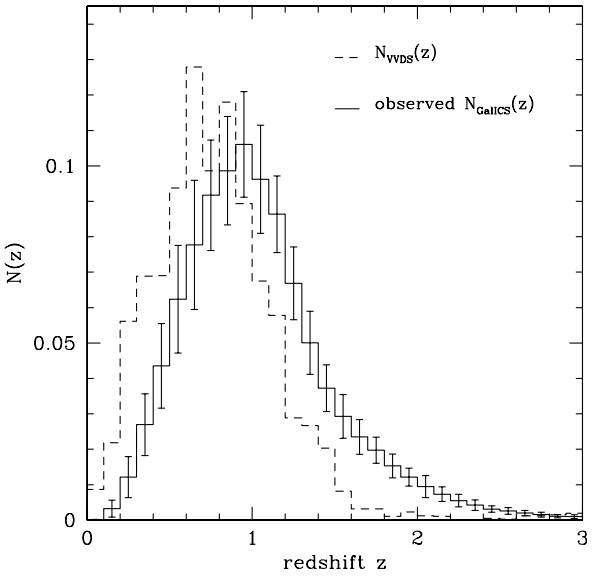

Fig. 4. Average redshift distribution in the 50 mock VVDS-02h surveys, normalized by the number of objects in each cone, compared to the redshift distribution of the observed VVDS galaxies. Note how the semi-analytic model of galaxy formation used to construct the *GalICS* simulations differs from the real data. This is not a concern for the purposes of this work: first, we are performing *internal* tests of the effect of observing biases and on their correction, which depends on the small-medium scale clustering properties. Second, when error bars are estimated for a specific redshift slice, their amplitude is re-normalized accordingly, to account for the different number of galaxies.

we consider (i.e. from 0.1 to 10 h^{-1} Mpc). The dispersion found among the 50 *GalICS* cones is thus expected to be a good estimate of cosmic variance. The mean number of galaxies with $17.5 < I_{AB} < 24$ in the artificial catalogs is 77 396. The average redshift distribution of these 50 cones is shown in Fig. 4, along with the VVDS first epoch $N(z)$ (Le Fèvre et al. 2005a).

We note that the redshift distribution of the simulated galaxies differs significantly from that observed by the VVDS for the real Universe. This is simply telling us that the semi-analytic galaxy formation model adopted to construct the *GalICS* simulations, while adequately reproducing a number of observed features (see Blaizot et al. 2005) is not 100% correct. This, however, is of no importance for the current analysis, as our main goal is to test the internal differences in the measured quantities when either the original parent sample or the final spectroscopic sample are observed. The accuracy of these tests depends essentially on the small-scale properties of the simulated galaxies (like the mean inter-galaxy separation and clustering), rather than on the global redshift distribution. Conversely, in the estimate of error bars the difference in absolute numbers between the real and simulated samples within a given redshift slice will clearly have to be taken into account.

3.2. CCD photometric mask

Bright (often saturated) stars represent a practical obstacle to accurate galaxy photometry and their diffused light can affect large areas of a CCD astronomical image. All such areas were excised from the VVDS photometric catalogs: there are no sources in these regions (McCracken et al. 2003). Similarly, a "dead" area in the 02h field has been produced by a beam of scattered light that crosses a large part of the field from North–East to South–West. In total, a few percent of the total area are lost due to these defaults. The information on these "holes" in the photometric catalog is stored in a FITS binary mask, with null values corresponding to dead pixels. We have used this mask on the mock samples to exactly reproduce the pattern of the observed data in our simulations.

3.3. Effect of galaxy angular sizes

In order to maximize the number of spectroscopic targets, the Super-SPOC software (Bottini et al. 2005) makes a choice of a targeted galaxy based also on the galaxy projected angular radius along the slit direction. This means that smaller galaxies are sometimes preferred as they allow the program to increase the number of targets. Any realistically simulated spectroscopic sample must take this into account. Therefore, we have computed for each simulated galaxy in *GalICS* a realistic angular radius, using the following procedure.

GalICS describes galaxies with three components: a disc, a bulge and possibly a nuclear starburst. For each of these, the model predicts the mass and a scale-length that assumes the disc is exponential while the other two spheroidal components follow a Hernquist profile (Hernquist 1990). We used these sizes to define an overall radius for each galaxy, which encloses 90% of the total mass. Assuming that light has the same distribution as mass, we then convert this radius to an apparent angular size, assuming the above-mentioned cosmology.

3.4. Artificial stars

The VVDS spectroscopic targets are selected purely on magnitude, $I_{AB} \leq 24$ and $I_{AB} \leq 22.5$ in the Deep and Wide parts of the survey, respectively, without any a priori star-galaxy separation. This avoids biases against compact galaxies and AGNs which may be introduced at faint magnitudes by unreliable star-galaxy classification based on morphology. Consequently, our spectroscopic sample is contaminated by stars. About 8.5% of the collected spectra in the VVDS-Deep are stars and are discarded (the exact number depending on galactic latitude can be as high as 20% in some cases for the "Wide" survey). These stars obviously have no impact on the clustering analysis. Their only effect is to reduce the total number of targeted galaxies, thus slightly affecting the overall statistics by increasing the expected variance. Since our aim here is to precisely quantify the biases and uncertainties on galaxy correlations computed from the final spectroscopic sample, and compare them to the original parent sample, we decided to also take into account this small contribution. We therefore added to the artificial survey fields a set of simulated stars.

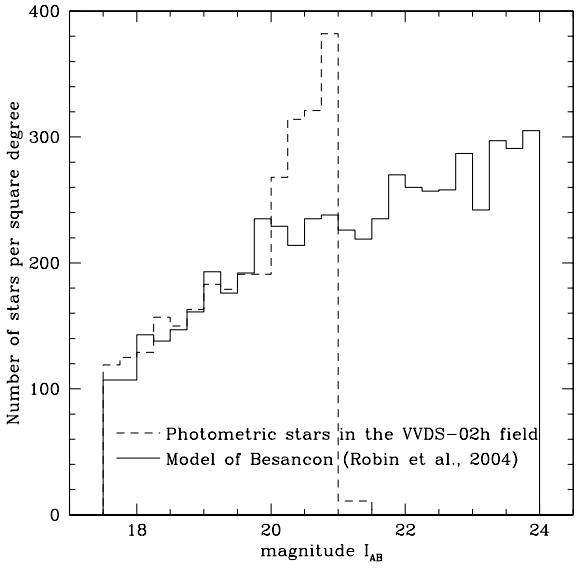

Fig. 5. Number counts of artificial stars added to the *GalICS* simulation, compared to the actual counts of stars in the VVDS-02h field, identified morphologically from the photometric data. The excess in the VVDS above $I_{AB} = 20$ is due to the inability of the morphological compactness criteria to discriminate stars from galaxies and QSOs at faint magnitudes. When this is taken into account, the models from Robin et al. (2003) reproduce very well the actual distribution of stellar objects in the VVDS.

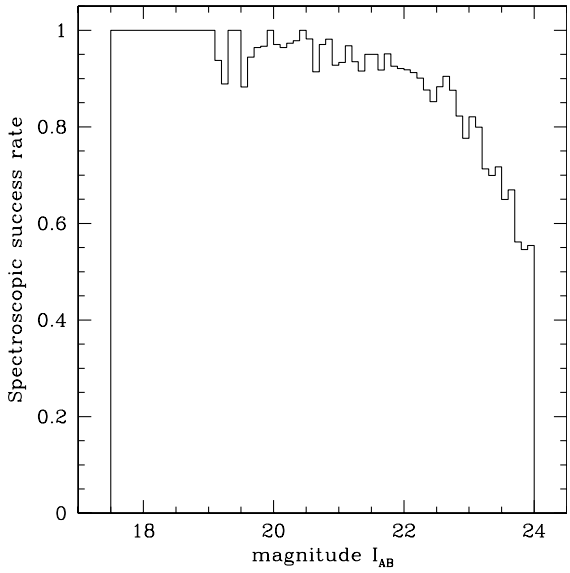

Fig. 6. Spectroscopic success rate per magnitude bin in the VVDS 02h field, including only those redshifts used for the clustering analysis.

Using the on-line tool of Robin et al. (2003)[2] we created a one-square-degree catalog of artificial stars with $17.5 \, I_{AB} \leq 24$, which was added to the artificial galaxy photometric catalogs. Figure 5 shows the number counts of the added stars, compared to the observed distribution at bright magnitudes in the 02h field (as identified by *S-extractor*, Bertin & Arnouts 1996). The observed excess above $I_{AB} = 20$ in the 02h field is the effect of mis-classified galaxies and QSOs, which also corroborates our choice of excluding any pre-selection for the VVDS spectroscopy, to avoid throwing these objects away.

As this parameter is used by VMMPS, apparent angular radii have also been assigned to artificial stars, using the observed distribution of stellar sizes in the 02h field, identified photometrically down to $I_{AB} = 21$ and spectroscopically at fainter magnitudes. This range of apparent stellar radii corresponds to the sizes of the point spread function ("seeing") at the faint Kron radii measured for stars by *S-extractor*.

3.5. Spectroscopic success rate

Objects selected by the slit-positioning code do not yet form the final redshift catalog. For some of the objects, redshift measurements are impossible, usually because of poor signal-to-noise. This incompleteness is clearly a function of magnitude. We define the spectroscopic success rate as the ratio of the number of redshifts used for clustering analysis to the total number of spectroscopically observed objects. Figure 6 shows the spectroscopic success rate as a function of magnitude, which corresponds in practice to the probability of measuring the correct redshift of a galaxy as a function of its magnitude in the current observational configuration. Overall, this shows that we are able to obtain a redshift for more than 80% of the targeted objects between $I_{AB} = 17.5$ and 24. We therefore apply this same probability function to our mock "observed" catalogs, rejecting the corresponding fraction of targeted objects. We make the simplifying assumption that the spectroscopic success rate is the same for all galaxy types.

3.6. VIMOS spectral resolution

The last point to be taken into account to produce a fully realistic mock redshift catalog is the resolution of the VIMOS spectrograph in the set-up used for the VVDS (Low-resolution RED Grism, $R \simeq 230$) which translates into a typical rms error on the measured redshift which is around $\sigma_{cz} \simeq 275 \, \mathrm{km \, s^{-1}}$. We therefore added to the final set of mock redshifts a Gaussian-distributed dispersion with the same rms and zero mean.

3.7. Overall properties of mock VVDS surveys

All of the steps described above have been applied to each of the 50 one-square-degree *GalICS* surveys, producing a corresponding number of mock redshift samples which reproduce with fidelity the lay-out, properties and biases of the first-epoch VVDS 02h sample.

Figure 7 shows that, despite the slight bias of SSPOC towards choosing smaller (and therefore fainter) objects, the redshift distribution $N(z)$ of the final spectroscopic samples is unbiased with respect to the original complete *GalICS* one-square-degree survey. The difference observed in Fig. 4 between the original and observed simulated cones is therefore

[2] The *Model of stellar population synthesis of the Galaxy* developed by Robin et al. (2003) produces a reliable catalog of stars with appropriate number counts and magnitudes in the visible and near-infrared spectral ranges in the Johnson-Cousins and Koornneef systems, respectively.

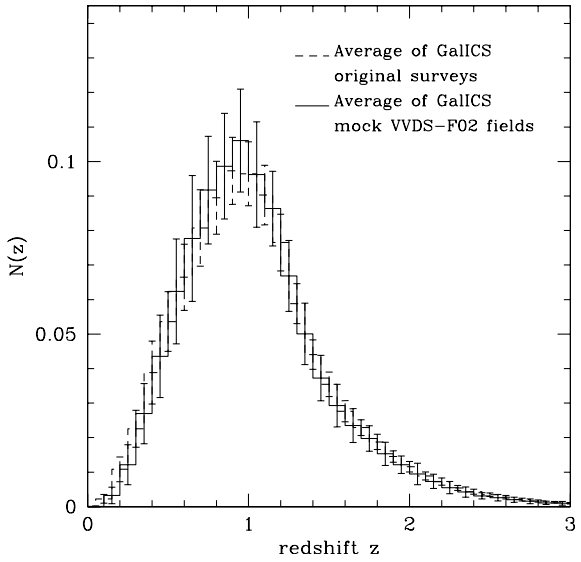

Fig. 7. Average redshift distribution in the *GalICS* mock catalogs before and after the full observing strategy is applied. No bias in the redshift distribution is observed.

only the result of the model of galaxy formation adopted for the simulation, and not of a selection effect. There was no way we could introduce, e.g., a stronger incompleteness in the final $N(z)$ at $z > 1$.

4. Two-point correlation statistics

4.1. General estimator

The two-point correlation function $\xi(r)$ is defined as the excess probability above random that a pair of galaxies is observed at a given spatial separation r (Peebles 1980).

It is the simplest statistical measurement of clustering, as a function of scale, and it corresponds to the second moment of the distribution. Various recipes have been proposed to estimate two-point correlation functions from galaxy surveys, in particular to minimize the biases introduced by the finite sample volume, edge effects, and photometric masks (Hamilton 1993; Landy & Szalay 1993). Here we adopt the Landy-Szalay estimator, that expresses $\xi(r)$ as

$$\xi(r) = \frac{N_{\rm R}(N_{\rm R}-1)}{N_{\rm G}(N_{\rm G}-1)}\frac{GG(r)}{RR(r)} - 2\frac{N_{\rm R}-1}{N_{\rm G}}\frac{GR(r)}{RR(r)} + 1. \quad (1)$$

In this expression, $N_{\rm G}$ and $N_{\rm R}$ are the mean density (or, equivalently, the total number) of objects respectively in the galaxy sample and in a catalog of random points distributed within the same survey volume and with the same redshift distribution and angular selection biases; $GG(r)$ is the number of independent galaxy-galaxy pairs with separation between r and $r+{\rm d}r$; $RR(r)$ is the number of independent random-random pairs within the same interval of separations and $GR(r)$ represents the number of galaxy-random pairs.

4.2. Redshift-space correlations

We know that the three-dimensional galaxy distribution recovered from a redshift survey is distorted due to the effect of peculiar velocities. For this reason, the redshift-space separation s differs from the true physical comoving separation r between two galaxies. Since random velocities affect only redshift and not position on the sky, the stretching occurs only radially. Redshift distortions can be measured and separated from true spatial correlations by computing the function $\xi(r_{\rm p}, \pi)$, where the separation vector of a pair of galaxies s is split into two components: π and $r_{\rm p}$, respectively parallel and perpendicular to the line of sight. Given two objects at redshifts z_1 and z_2, with observed radial velocities $v_1 = cz_1$ and $v_2 = cz_2$ (c being the speed of light), we can define (Fisher et al. 1994) the line of sight vector $\boldsymbol{l} \equiv (\boldsymbol{v1} + \boldsymbol{v2})/2$ and the redshift difference vector $\boldsymbol{s} = \boldsymbol{v1} - \boldsymbol{v2}$, and also:

$$\pi \equiv \frac{\boldsymbol{s}\cdot\boldsymbol{l}}{H_0|\boldsymbol{l}|}, \qquad r_{\rm p}^2 \equiv \frac{\boldsymbol{s}\cdot\boldsymbol{s}}{H_0^2} - \pi^2. \quad (2)$$

Equation (1) can be generalized to the case of $\xi(r_{\rm p}, \pi)$, if we count the number of pairs in a grid of bins $\Delta r_{\rm p}$ and $\Delta\pi$ instead of singular bins Δr or Δs.

Observed distortions in galaxy surveys can be separated into two main contributions: on small scales, the distortion is dominated by random internal velocities in groups and clusters, causing a stretching of $\xi(r_{\rm p}, \pi)$ along the π direction (the so-called "fingers of God" effect). On large scales, on the other hand, $\xi(r_{\rm p}, \pi)$ contours tend to be flatter, due to coherent infall of galaxies onto large-scale overdensities, known as the "Kaiser effect" (Kaiser 1987). The latter is a weak effect and needs very large samples to be seen with sufficient accuracy, as shown by the 2dF survey (Hawkins et al. 2003).

4.3. Projected correlation function $w_{\rm p}(r_{\rm p})$

We can recover the real-space correlation function $\xi(r)$ by projecting $\xi(r_{\rm p}, \pi)$ along the line of sight, onto the $r_{\rm p}$ axis. In this way we integrate out the dilution produced by the redshift-space distortion field and obtain a quantity, $w_{\rm p}(r_{\rm p})$, which is independent of the redshift-space distortions:

$$w_{\rm p}(r_{\rm p}) \equiv 2\int_0^\infty \xi(r_{\rm p}, \pi){\rm d}y = 2\int_0^\infty \xi_\circ\left[(r_{\rm p}^2 + y^2)^{1/2}\right]{\rm d}y. \quad (3)$$

In the right-hand side of the equation, $\xi_\circ$ is simply the usual real-space two-point correlation function $\xi(r)$, evaluated at the specific separation $r = \sqrt{r_{\rm p}^2 + y^2}$. If we now assume a power-law model

$$\xi(r) = \left(\frac{r}{r_0}\right)^{-\gamma}, \quad (4)$$

with γ being the slope of the correlation function and r_0 the correlation length, the integral can be computed analytically, giving as a result

$$w_{\rm p}(r_{\rm p}) = r_{\rm p}\left(\frac{r_0}{r_{\rm p}}\right)^\gamma \frac{\Gamma\left(\frac{1}{2}\right)\Gamma\left(\frac{\gamma-1}{2}\right)}{\Gamma\left(\frac{\gamma}{2}\right)}, \quad (5)$$

where Γ is Euler's Gamma function.

5. Error estimate and fitting technique

5.1. Error bars on correlation functions

Ideally, if the studied data set consisted of a large enough number of statistically independent pairs, such that the central limit theorem applies, then the distribution of estimates of ξ in an ensemble of similar samples should be Gaussian. The 1σ uncertainty – the "cosmic error"– in ξ would then be the square root of its variance $\langle\Delta\xi^2\rangle$ (Peebles 1973). However, the theoretical expression for $\langle\Delta\xi^2\rangle$ depends on the poorly known and difficult to measure four-point correlation function. Moreover, since the measured ξ is not exactly coincident with the theoretical ξ, we expect its uncertainty to be also somewhat different from the value provided by the theory. This effect is known as a cosmic bias.

A few different ways of estimating errors on two-point correlation functions have been used in the literature (for a wider discussion, see e.g. Hamilton 1993; Fisher et al. 1994; Bernardeau et al. 2002). The case closest to the ideal situation is when the survey is large enough that it can be split into a number of sub-samples. Correlations are then estimated independently for each of these, and error bars for the parent sample computed as the rms values. This has been for example the case of the angular correlation function from the APM survey (e.g. Maddox et al. 1990). However, the number of subsamples cannot be large, otherwise the explored scales will be significantly reduced with respect to the parent survey. The consequence is that the variance is typically overestimated and these represent usually upper limits to the true errors.

Simple Poissonian errors (e.g. proportional to the square root of the total number of galaxy pairs in each bin) underestimate the error bars substantially. Statistical corrections were proposed (Kaiser 1986) by multiplying Poissonian errors by a factor $1+4\pi nJ_3$, with n being the number density of objects and $J_3 = \int^{r_j} r^2\xi(r)\mathrm{d}r$, where we assume that the actual correlation function vanishes for $r \geq r_j$. However, this method also tends to give relatively small errors (Fisher et al. 1994).

Over the last twenty years a widely used method has been the so-called "bootstrap resampling" (Barrow et al. 1984). It is based on the idea of "perturbing" the data set, by randomly creating a large number of comparable "pseudo data-sets", which differ only slightly from the original sample. If this contains N objects, then each bootstrap sample is created selecting N of these, but allowing for multiple selections of the same object. This means that some objects will not be included in one given pseudo data-set, while others will be counted twice or three times. This is a good test of the robustness of measured correlations, especially on large scales where having a large number of pairs does not always mean a robust measurement: consider for example the case of a single isolated galaxy at a separation of $\bar{r}$ from a cluster containing 1000 galaxies. $\xi(\bar{r})$ will contain a large number of pairs, however only one will be independent. On the other hand, bootstrap errors often tend to over-estimate the theoretical variance $\langle\Delta\xi^2\rangle$. In general, however, despite debates on their theoretical justification, they have represented a practical way to obtain error bars in correlation analysis which are not far from the true ones.

The use of bootstraping became less and less popular in recent years, with the advent of large N-body simulations, reproducing the matter distribution over significant volumes of the Universe. Coupled to physically sound definitions of "galaxies", these allowed the construction of sets of independent mock surveys, from which ensemble errors could be computed from the scatter in the different catalogs. This is the same technique used to construct our VVDS mock surveys. Clearly, a good match is necessary between the volume and resolution of the simulation, on one side, and the depth and size of the survey on the other. Furthermore, the power spectrum of the simulation must provide a realistic description of long waves, so to properly include cosmic variance. Progress both in our knowledge of structure on the largest scales and in the size and resolution of N-body simulations has improved on early applications of this technique (Fisher et al. 1994). For this reason, since the *GalICS* simulations are available, we could use this as our main method for error estimation.

However, as we detail below, the covariance matrix reconstructed from the simulations cannot be applied in a straightforward way to the observed data. Indeed, our fitting technique, discussed below, handles the covariance matrix to properly account for bin-to-bin correlations when fitting correlation functions: when the covariance matrix extracted from the set of 50 mock VVDS surveys is used (after proper normalization of the average values), the fit is often unstable. In other words, the covariance matrix produced by the ensemble of mock surveys, although providing sufficiently realistic diagonal elements, has off-diagonal non-zero values which differ from those pertaining to the data sample (which of course are unknown). For this reason, we modified our strategy and resort to the bootstrap technique *to estimate the bin-to-bin covariance*. This means that our error bars on the estimated correlation functions are obtained via the more reliable scatter between the mock surveys, but a bootstrap is used to estimate the off-diagonal terms of the covariance matrix.

5.2. Fitting correlation functions

It is well known that fitting of correlation functions like $\xi(s)$ or $w_\mathrm{p}(r_\mathrm{p})$ cannot be performed via the standard least-squared method, due to the correlation existing among the different bins. The procedure we adopted to estimate the power-law parameters of $\xi(r)$, r_0 and γ from the projected function $w_\mathrm{p}(r_\mathrm{p})$, using Eq. (5) follows Fisher et al. (1994) and Guzzo et al. (1997), with some specific differences that are described in the following.

Let us consider a given redshift slice $[z_1 - z_2]$. Within this same interval, we estimate the correlation function $\xi(r_\mathrm{p}, \pi)$ from: 1) 50 mock VVDS surveys; 2) the real VVDS data; 3) N_boot (typically 100) bootstrap resamplings of the VVDS data. We then compute, for each of these estimates, $w_\mathrm{p}(r_\mathrm{p})$, projecting $\xi(r_\mathrm{p}, \pi)$ along the line of sight (Eq. (3)), with an upper integration limit π_max, chosen in practice so that it is large enough to produce a stable estimate of w_p. Similarly to other authors (see e.g. Guzzo et al. 1997), we find $w_\mathrm{p}(r_\mathrm{p})$ quite insensitive to the choice of π_max in the range of

$15\,h^{-1}\,\mathrm{Mpc} < \pi_{\max} < 25\,h^{-1}\,\mathrm{Mpc}$ for $r_\mathrm{p} < 10\,h^{-1}\,\mathrm{Mpc}$. Too small a value for this limit would miss small-scale power, while too large a value has the effect of adding noise into w_p. After a set of experiments we have chosen $\pi_{\max} = 20\,h^{-1}\,\mathrm{Mpc}$.

In the following, we call $w_\mathrm{p}^k(r_i)$ the value of w_p, computed at $r_\mathrm{p} = r_i$ in the cone k, where $1 \le k \le N_\mathrm{GalICS} = 50$ if we consider the *GalICS* data or $1 \le k \le N_\mathrm{boot}$ if we consider the bootstrap data. If not otherwise mentioned, $N_\mathrm{boot} = 100$ is used.

Whether we consider the mock or bootstrap samples, we can always compute the associated covariance matrix, $\mathbf{C}$, between the values of w_p in ith and kth bins:

$$\mathbf{C}_{ik} = \left\langle \left(w_\mathrm{p}^j(r_i) - \langle w_\mathrm{p}^j(r_i)\rangle_j\right)\left(w_\mathrm{p}^j(r_k) - \langle w_\mathrm{p}^j(r_k)\rangle_j\right)\right\rangle_j, \quad (6)$$

where "$\langle\rangle_j$" indicates an average over all bootstrap or mock realizations. When the correlation function is computed from a finite sample, the values of $\xi(r)$ (or $w_\mathrm{p}(r)$) at different separations are not independent[3] For this reason one cannot use a straightforward χ^2 minimization – which assumes that all bins are independent and that the errors follow the Gaussian distribution – to find the best-fit parameters of a model to the observed data. However, $\mathbf{C}$ is symmetric and real and therefore can be diagonalized by a unitary transformation if its determinant is non-vanishing. In practice, the estimated functions are oversampled, $\mathbf{C}$ is not singular and therefore can be inverted by a simple Cholesky decomposition (Numerical Recipes, Press et al. 1992, Volume 1, Chapter 2)[4]. Then, if we now call $\mathbf{H} = \mathbf{C}^{-1}$, we can fit $w_\mathrm{p}^\mathrm{VVDS}$ by minimizing a generalized χ^2, which is defined as

$$\chi^2 = \sum_{i=1}^{N_\mathrm{D}}\sum_{j=1}^{N_\mathrm{D}}\left(w_\mathrm{p}^\mathrm{mod}(r_i) - w_\mathrm{p}^\mathrm{VVDS}(r_i)\right) H_{ij}\left(w_\mathrm{p}^\mathrm{mod}(r_j) - w_\mathrm{p}^\mathrm{VVDS}(r_j)\right), \quad (7)$$

as a function of the two free parameters r_0 and γ of $w_\mathrm{p}^\mathrm{mod}(r_\mathrm{p})$.

In principle, the complete process could be done using only our set of 50 mock VVDS surveys. In practice, as explained above, the bin-to-bin covariance obtained from the *GalICS* mock samples does not provide a statistically stable matrix to be used with the generalized χ^2 method. Therefore, we most appropriately used the covariance matrix obtained from the N_boot bootstrap resamplings of the galaxy data set.

This provides the best solution for $(r_0, \gamma)_\mathrm{data}$ that minimizes the error contour $\chi^2_\mathrm{boot}(r_\mathrm{p}, \gamma)$. At the same time, however, we use 50 mock surveys to obtain the most realistic error contours $\chi^2(r_\mathrm{p}, \gamma)$ on our estimated $(r_0, \gamma)_\mathrm{data}$, as these – unlike bootstrap errors – include cosmic variance.

The final error contours, therefore, are obtained fitting the mean of the 50 w_p mock VVDS surveys, using a covariance matrix computed from the same 50 w_p. This process provides a solution for $(r_0, \gamma)_\mathrm{GalICS}$ associated with the error contours $\chi^2_\mathrm{GalICS}(r_\mathrm{p}, \gamma)$. We then re-center these contours around $(r_0, \gamma)_\mathrm{data}$ with the renormalization $r_\mathrm{p} \leftarrow r_\mathrm{p} \times (r_0^\mathrm{GalICS}/r_0^\mathrm{data})$ and $\gamma \leftarrow \gamma \times (\gamma^\mathrm{GalICS}/\gamma^\mathrm{data})$.

To take into account the different $N(z)$ of GalICS and VVDS, we multiply the error contour χ^2_GalICS computed for each redshift slice by a factor $N_\mathrm{VVDS}/N_\mathrm{GalICS}$, where N_VVDS is the number of VVDS galaxies and N_GalICS is the number of *GalICS* galaxies in this redshift slice.

The error bars computed as above for each $w_\mathrm{p}(r_i)$ value correspond to the rms of the 50 $w_\mathrm{p}^k(r_i)$, normalized to the data.

6. Biasing effects and their removal

We now quantitatively establish the impact of the VVDS selection effects on the measured correlations and the accuracy of our correcting scheme, using the *GalICS* mock samples.

6.1. Impact on angular correlations

As we have seen in the previous section, the biases and selection effects due to the observing strategy and instrumental limitations affect the properties of the angular distribution of objects, with respect to a random sub-sampling of galaxy clustering process. It is therefore the angular correlation function $\omega(\theta)$ that will primarily reflect these biases. Clearly, there is no specific scientific reason to measure the angular correlation function from the spectroscopic sample, as this can be done more easily and with much greater confidence using the full VVDS photometric catalog (McCracken et al. 2003). $\omega(\theta)$ allows us to illustrate the level of distortions introduced by our angular selection function.

To this end, Fig. 8 shows the angular correlation function computed from one mock VVDS redshift survey without correcting for these effects (i.e. using a random sample which simply follows the geometrical borders of the galaxy sample, as one would do for a homogeneous angular selection), compared to that of the original mock catalog. We used the angular version of the Landy-Szalay estimator (Eq. (1)), without taking into account any incompleteness on any scales. The comparison to the parent survey $\omega(\theta)$ reveals the very strong distortions introduced over a wide range of angular scales.

6.2. Correction scheme

The biases discussed so far involve introducing two types of corrections which we discuss in detail in this section.

1) *Global correction.* To account for the effects of uneven boundaries and varying sampling rate we construct a random catalog, which consists of the same number of separately created pointings as the galaxy sample, thus reproducing the global "exposure map" (i.e. number of multiple passes over a given point of the sky) and the corresponding large-scale surface density variations of the galaxy redshift sample. The holes and excised regions in the photometric sample are similarly taken into account by applying the same binary mask to the random sample. These first-order corrections account already

[3] For example, imagine that one galaxy is removed from the sample: this galaxy contributes pairs at many different separations, thus affecting virtually all bins in the correlation function.

[4] Note that if the number of bins we want to fit, i.e. the size of the matrix, were greater or equal to the number of realizations then, even if the matrix remains symmetric, the vectors would not be independent and the matrix $\mathbf{C}$ could not be inverted.

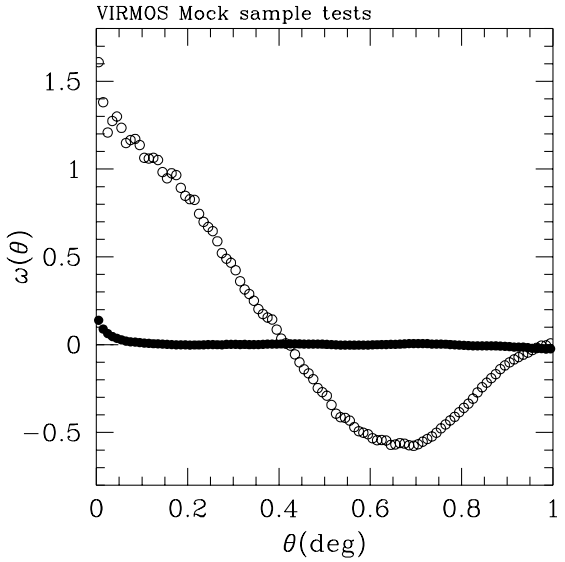

Fig. 8. Impact of the observational process on the estimate of the angular two-point correlation function $\omega(\theta)$ for one mock VVDS survey (open circles), compared to that of the original parent field (filled circles), for one mock VVDS cone. The large distortion, introduced by the observing strategy affects practically all angular scales.

for most of the observational biases. When taken into account, they reduce most of the negative effects of the observing strategy on the correlation functions, in particular the global overestimation of correlation functions (see Figs. 9–11).

2) *Small scale correction.* What remains to be corrected is the slight bias introduced by the slit-positioning software and the mechanical limitations (slit size, closeness of slits and so forth). We have seen that the SSPOC selection is not an entirely random sampling of the actual angular distribution of objects, but rather a more homogeneous sub-set, preferentially concentrated along specific rows. This selection affects primarily the small-scale values of the correlation function, corresponding to the typical slit size: with only one spectroscopic pass, pairs of galaxies with separation smaller than the slit size will always have only one galaxy observed, and thus their contribution to ξ will be lost. With repeated passes this problem is alleviated, as the software chooses each time different objects (except for a small number of objects observed twice for error checking purposes). Using the full 2D information available from the parent photometric catalog (that tells us how many galaxies on the sky have been missed in the spectroscopic sample), we developed a weighting scheme that weighs each targeted galaxy proportionally to its "representativity" in terms of local angular pair density.

Let us therefore consider a circular region of radius θ_w around a galaxy i located within a specific redshift slice k, and define inside θ_w the following quantities:
$n_{\rm gal}(i)$ – the number of galaxies in the parent photometric catalog;
$n_z(i)$ – the number of galaxies with measured redshift;
$n_{\rm in}(i)$ – the subset of these belonging to the same redshift slice as the central galaxy;
$n_{\rm exp}(i)$ – the number of galaxies expected to belong to the same redshift slice, which can be written as

$$n_{\rm exp}(i) = n_{\rm in}(i) + n_{\rm rem}(i), \tag{8}$$

with $n_{\rm rem}$ being the fraction of unobserved neighboring galaxies in the parent photometric catalog expected to belong to the same redshift slice. This number can be written as

$$n_{\rm rem}(i) = [n_{\rm gal}(i) - n_z(i)] * P_{\rm slice}, \tag{9}$$

where $P_{\rm slice}$ is the probability that a generic measured galaxy belongs to that specific redshift slice. Here one can make the reasonable assumption that the observed redshift distribution N_z is sufficiently well sampled as to provide, when averaged over a suitably chosen radius $\theta_{\rm A}$, an unbiased estimate of $P_{\rm slice}$ for any kth slice as

$$P_{\rm slice} = \frac{N_{z,k}(<\theta_{\rm A})}{N_{z,{\rm total}}(<\theta_{\rm A})}. \tag{10}$$

The choice of $\theta_{\rm A}$ is clearly critical, as it has to be large enough to allow a proper sampling of existing structures along the line of sight (and thus minimize the noise introduced by the weight), but also small enough not to dilute the effect of single structures within one redshift slice. In practice, given the current size of the 02h field (~0.5 square degrees), we have obtained the best results using $\theta_{\rm A} = 30'$, which encloses virtually the entire field. Note also that $n_{\rm gal}(i)$, i.e. the number of galaxies in the parent catalog, will be given by $n_{\rm gal}(i) = n_{\rm all}(i) * f_{\rm gal}$, with $f_{\rm gal}$ being the probability that a randomly chosen object from the photometric catalog is not a star but a galaxy and $n_{\rm all}(i)$ – the number of all locally observed objects in this catalog. For the actual VVDS 02h field, this probability has been estimated to be $f_{\rm gal} = 0.92$.

The construction of the actual weight to recover the loss of small-scale pairs produced essentially by the proximity bias is not unequivocal. After several experiments with weighting by local densities (of expected vs. observed spectra), we obtained the best results weighting by pairs. The two-point correlation function being a pair-weighted statistic, we constructed our weight $w(i)$ for a given galaxy i from the ratio of the expected to the measured number of pairs within θ_w. Specifically, if one wants the local angular pair density to be conserved, each pair should be counted as:

$$w(i) * w(j) = \frac{n_{\rm exp}(i) * (n_{\rm exp}(j) - 1)}{n_{\rm in}(i) * (n_{\rm in}(j) - 1)}. \tag{11}$$

And, consequently, a single object is assigned a weight

$$w(i) = \sqrt{\frac{n_{\rm exp}(i) * (n_{\rm exp}(i) - 1)}{n_{\rm in}(i) * (n_{\rm in}(i) - 1)}}. \tag{12}$$

To define the optimal angular size θ_w defining the "neighborhood" of a galaxy, we experimented with different values in the range $5''$ to $1'$. Not surprisingly, the best correction is obtained for θ_w in the range $30{-}45''$, which is comparable to the length of the VIMOS spectra as projected on the sky. In all computations presented here, we adopted the value $\theta_w = 40''$.

The following sections will present the results of extensive tests of this correction scheme, based on the *GalICS* mock VVDS surveys.

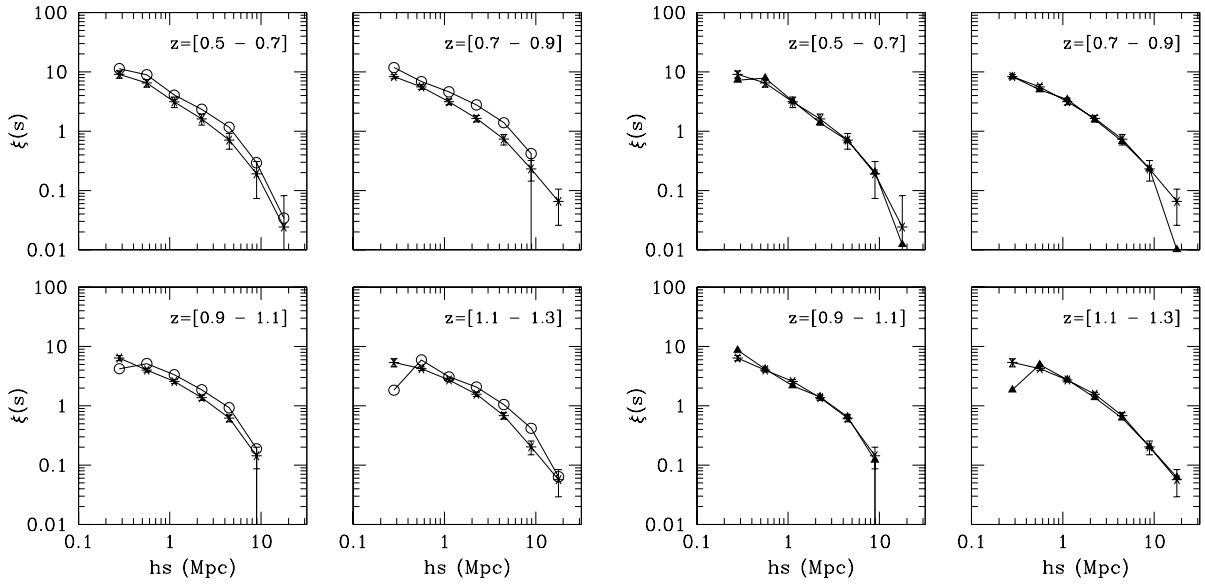

Fig. 9. Redshift-space two-point correlation function $\xi(s)$ for one mock VVDS-02h field, computed in four redshift bins. The true $\xi(s)$ computed for the whole parent sample (stars) is compared to that measured from the "observed" sample, first without any correction (open circles, *left four panels*) and then applying our correction scheme (triangles, *right four panels*). Error bars are the 1σ ensemble rms among the 50 VVDS mock samples.

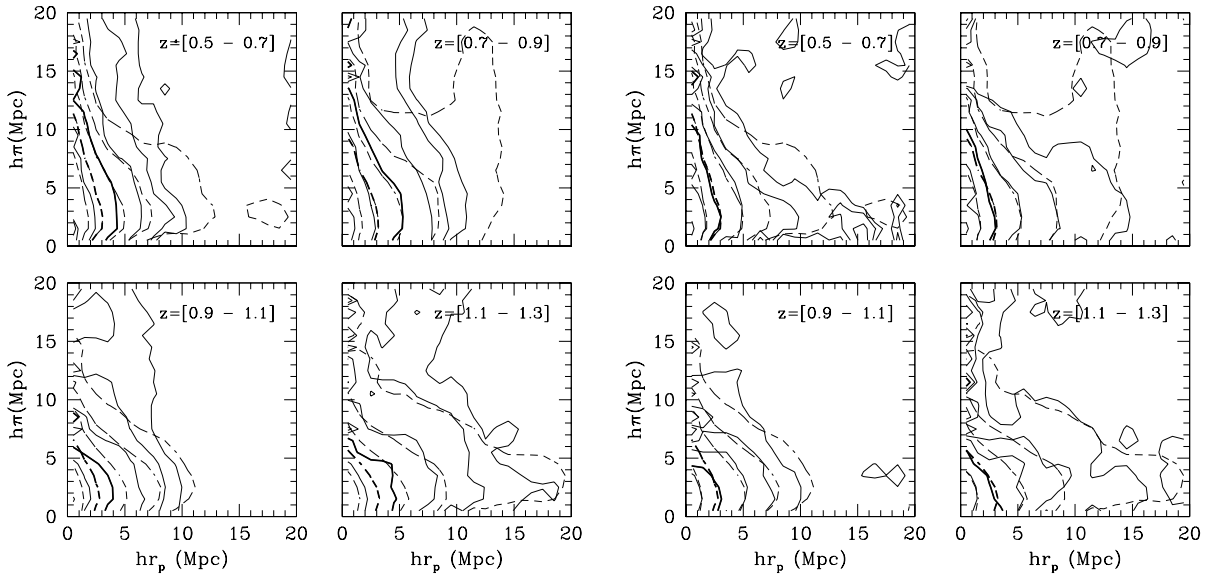

Fig. 10. Same as Fig. 9, but for the $\xi(r_\mathrm{p}, \pi)$ correlation function. The contours correspond to values for $\xi(r_\mathrm{p}, \pi)$ of 0.4, 1 (bold), 2.0, 5.0. Dashed lines refer to the complete mock sample, while solid ones describe the sample after applying the VVDS selection function.

6.3. Application to redshift-space correlations

We have applied the manipulations presented in the previous section to our mock VVDS 02h surveys and compared the results to those obtained from the whole 1deg $\times$ 1 deg mock fields. The results are shown in Figs. 9–11 for the same mock sample used for measuring $\omega(\theta)$ (Fig. 8), split into 4 redshift bins. In each of these figures, comparison of the the four left to the four right panels demonstrates the effect of the overall correction. In general, in redshift space the effect of the observational biases is much less severe, being diluted by the unaffected clustering measured along the line of sight. Still, we see how a proper estimate does require a correction.

Looking at $\xi(s)$ (Fig. 9), we see that the correction introduced by our scheme is in general very good. The full bi-dimensional correlation function $\xi(r_\mathrm{p}, \pi)$ (Fig. 10) shows the effect in more detail, indicating also that the impact of the angular bias on spatial correlations depends on redshift. This is to be expected, given that a fake inhomogeneity at a given angular scale affects larger spatial scales at larger redshifts. However, as seen from the four right panels the bulk of the problem is corrected by our technique.

Finally, the corresponding projected function, $w_\mathrm{p}(r_\mathrm{p})$, which is the one that will be fitted to estimate the real-space correlation length and slope, (Le Fèvre et al. 2005), does not show any significant systematic effect, nor scale-dependent

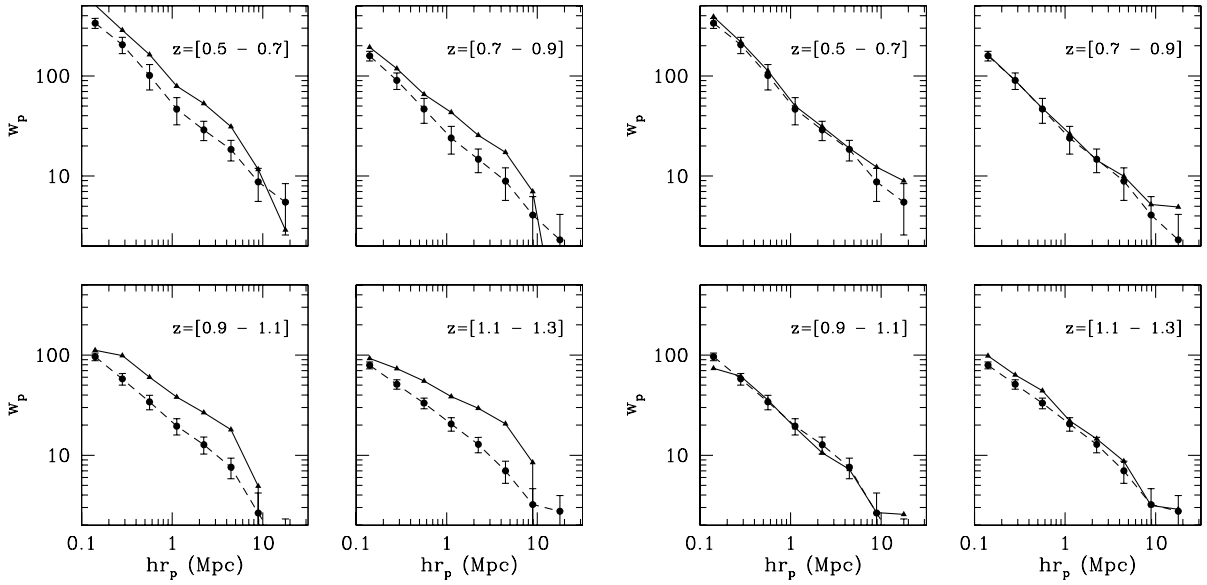

Fig. 11. Same as Figs. 9 and 10, but for the projected function $w_p(r_p)$, measured before (dashed line) and after (solid line) the full observing strategy has been applied. This comparison shows that our method is able to properly recover $w_p(r_p)$. We note, however, that, being closely related to the angular function, $w_p(r_p)$ remains the most sensitive among the 3D correlation functions to the observational biases and the most difficult to recover properly in all r_p bins.

bias (see also Sect. 6.4, below), if one excludes a residual effect in the highest-redshift bin (which may be specific of the mock sample used).

6.4. Accuracy in recovering r_0 and γ

Let us now evaluate more quantitatively how well the weighting scheme is able to recover the correct values of the two parameters of $\xi(r)$, r_0 and γ. Figure 12 plots the projected correlation function w_p, computed for one of the VVDS mock cones, together with the measured best fit values of r_0 and γ. The error contours are estimated from the variance of the 50 mock surveys as described previously and their size depends mainly on the number of galaxies within each bin. Figure 13 shows that the evolution of clustering we "observe" in this specific simulated VVDS cone agrees quite well with its parent sample.

Of course, due to cosmic variance, the values of r_0 and γ differ between different simulated cones. Figure 14 shows the spread of these parameters among all the 50 mock VVDS surveys and their parent catalogs, for a representative redshift bin (z = [0.5–0.7]). This behavior is similarly seen in the other redshift bins, indicating an increased spread in the parameter estimates in the "observed" catalogs, an effect easily explained in terms of the smaller number of objects. Figures 12 and 14 also indicate that at the end of our correction process any possible systematic effect is reduced to less than 5%, a value always significantly smaller than the uncertainty due to cosmic variance which is of the order of 15–20%.

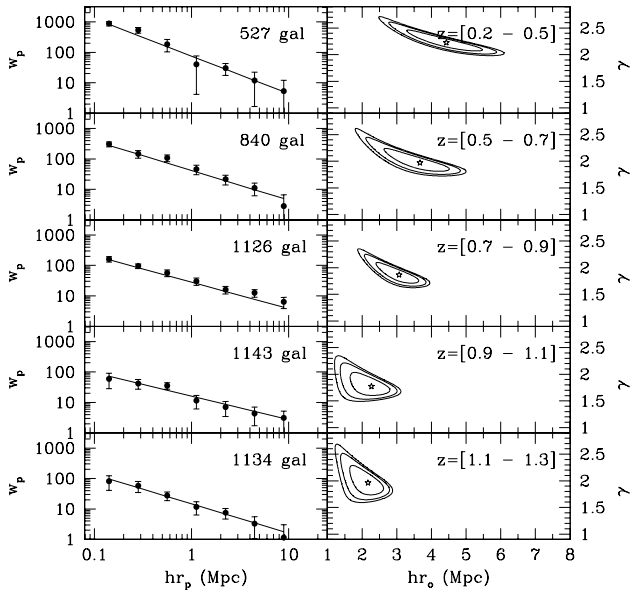

Fig. 12. Evolution of the projected function $w_p(r_p)$ (*left column*) and the corresponding best-fit parameters of $\xi(r)$, r_0 and γ (*right column*), as seen in one of the VVDS mock surveys. Error bars are computed as explained in the text, while error contours on the fit parameters are obtained taking into account the full covariance matrix. The 68.3%, 90% and 95.4% joint confidence levels are defined as in Numerical Recipes (Numerical Recipes, Press et al. 1992, chapter 15.6) in terms of the corresponding likelihood intervals that we obtain from our fitting procedure (see Sect. 5.2).

6.5. Tests of VVDS observing strategy

In this section we want to discuss from a more general perspective (i.e. not limited to the current status and lay-out of the 02h field) how the accuracy of correlation measurements can depend on the number of multiple spectroscopic pointings ("passes") that are dedicated to a specific area. In other words: are multiple passes increasing – as expected – the accuracy of correlation function measurements, not only thanks to the increased statistics, but also because of the improved sampling

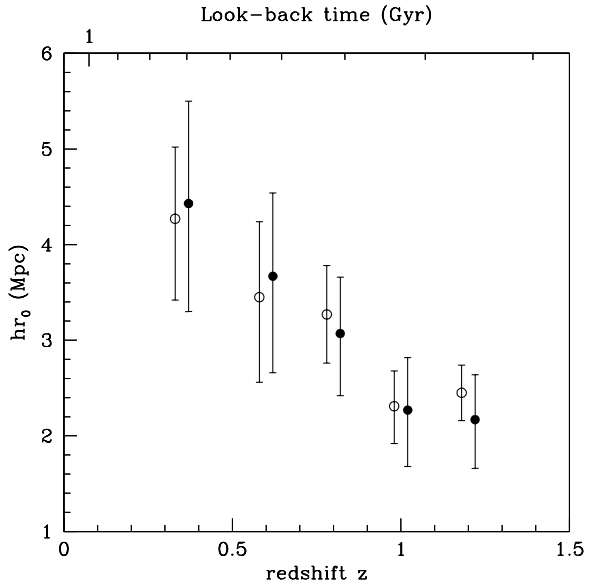

Fig. 13. Evolution of r_0 in a VVDS mock survey (filled circles), compared to that of its parent catalog (open circles). Error bars are as explained in the text. The "true" and "measured" values of r_0 are very consistent within the error bars, providing an *internal* proof of the quality of our correction scheme.

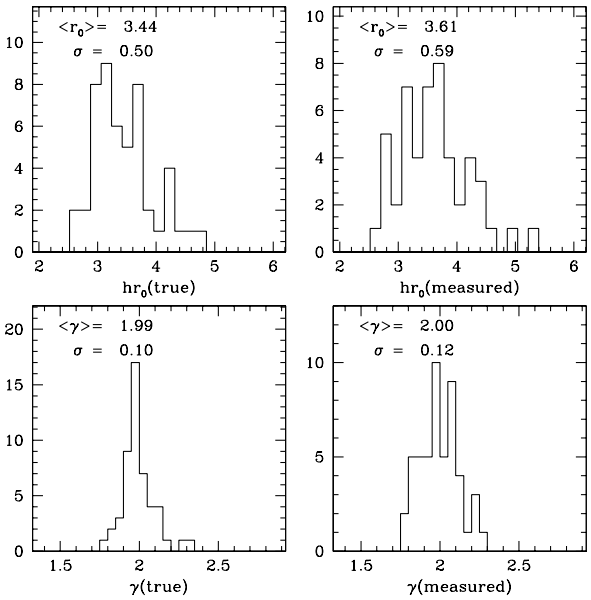

Fig. 14. Histograms of the measurements of r_0 and γ in the redshift bin [0.5–0.7] (chosen as a representative case), among the 50 mock catalogs, for the full cones (*left column*) and for the observed samples (*right column*), where the full weighting scheme has been applied. The ensemble averaged values of r_0 and γ are indicated in each panel, together with their rms error.

of the clustering process? And how is our correcting scheme performing when handling a very sparse (one pass) or a more densely sampled area? This is clearly an interesting question for the future development of the VVDS, or other surveys, as these tests can indicate what strategy could be more efficient. One would like to estimate the fraction of galaxies necessary to recover the correlation signal to a certain level of accuracy.

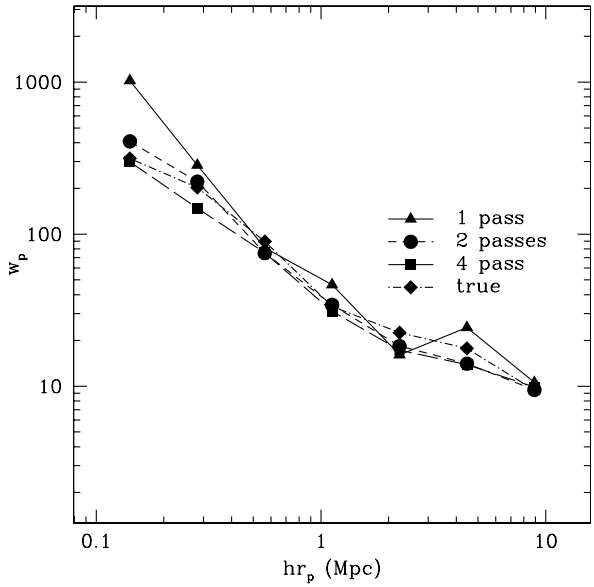

Fig. 15. Measured $w_p(r_p)$ in the case of different number of passes over the same field. When the field is observed only once we are clearly not able to properly recover properly $w_p(r_p)$ on the smallest scale. When we observe the field more times the recovery is much better also on the small scales.

This, translated to the VVDS, implies determining how many spectroscopic "passes" with VIMOS are necessary. Note that the answer is not trivial, since multiple pointings over the same area are usually dithered (i.e. shifted by an amount at least larger than the central "cross", i.e. 2′), and thus a larger number of passes over the same area, while improving the sampling, introduces also a more complex mean density pattern, as explained in Sect. 2.1.

Tests have been performed creating a grid of six pointings, spaced with the same step as the real VVDS ones in the VVDS-10h field. The second pass was then arranged over a grid shifted by 2′ in right ascension and declination. The pointings of both passes have then been "observed" once again with a different selection of objects for spectroscopy. At the end (maximum coverage), this resulted in an area of 0.3624 square degrees, mostly uniformly covered but with small patches of sky that were observed either three, two or one times or remained unobserved. The results for $w_p(r_p)$ and $\xi(s)$ are shown in Figs. 15 and 16, respectively.

The projected correlation function w_p is fairly well recovered almost independently of the sampling density. For a single pass, power is not recovered properly at scales below 0.6 h^{-1} Mpc, since there is in practice no pair (even biased) to be "corrected" in a proper statistical way by our scheme.

The case of $\xi(s)$ (Fig. 16) shows even more clearly the difficulty of recovering very small scale pairs with only one pass: in this case, there is an intrinsic low-scale limitation (complete lack of pairs), which cannot be fully overcome by the correcting scheme. The figure shows, for example, that while a linear bin between 0 and 1 h^{-1} Mpc is already sufficient to recover the correct clustering amplitude even with one pass, smaller logarithmic bins below 1 h^{-1} Mpc are inadequate and suffer from the lack of measured pairs.

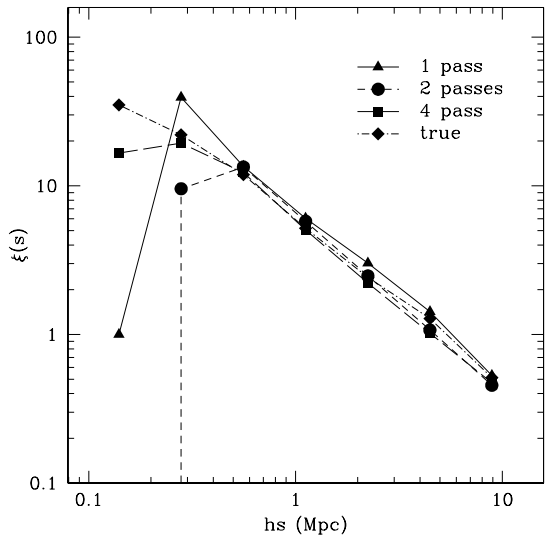

Fig. 16. Measurements of $\xi(s)$ for a different number of observing "visits" over the same field.

We conclude that even in the fields that were observed only with one spectroscopic observation, sampling about 15% of the photometric targets down to $I_{AB} = 24$, the two-point correlation function can be measured quite well for separations $1 \leq r \leq 10\ h^{-1}$ Mpc. The results confirm, however, that observing fields four times, sampling about 40% of the population as in the deep part of the VVDS, provides the possibility of more precise measurements on scales down to $0.1\ h^{-1}$ Mpc.

7. Summary and conclusions

One of the key goals of the VVDS survey is to measure the evolution of the galaxy clustering from the present epoch up to $z \sim 2$ and larger. To study in detail the error budget of $\xi(r)$ measurements in the VVDS survey, we have generated a set of mock catalogs using the GalICS model of semi-analytic galaxy formation. The geometry of the VVDS survey on the sky is complex due to the observing strategy. The resulting selection function substantially affects the angular correlation properties of the clustering of the observed galaxies. We demonstrate that the correlation observed in redshift space is much less affected and that the bias introduced by the observing strategy can be largely removed using the correcting scheme we propose in this paper.

We conclude that, for the first epoch VVDS data, we can expect to measure $\xi(s)$ and $w_{\rm p}(r_{\rm p})$ to better than 10% on scales $1 \leq r \leq 10\ h^{-1}$ Mpc, and better than 30% below $1\ h^{-1}$ Mpc. Results obtained from the GalICS simulations indicate that the two-point correlation functions computed from the First Epoch VVDS should suffer only from a modest cosmic variance of $\simeq$15−20%. These results suggest that after the final selection of objects for spectroscopy the variance becomes twice as large as the variance of the underlying parent galaxy field in the same area. We expect, in each redshift slice $\Delta z \simeq 0.2$ in the redshift range $z = [0.2, 2.1]$, to measure r_0 and γ with an accuracy better than 15−20%. We show that any residual systematic effect in the measurements of r_0 and γ is below 5%, i.e. a value much smaller than the cosmic errors.

The actual measured clustering properties of galaxies in the VVDS survey, using the framework outlined in this paper, are presented in Le Fèvre et al. (2005b) and in forthcoming papers.

Acknowledgements. We thank the *GalICS* group for access to their simulations, S. Colombi for providing a first set of mock *n*-body samples early in the development of this work and for useful discussions. This research has been developed within the framework of the VVDS consortium and has been partially supported by the CNRS-INSU and its Programme National de Cosmologie (France), and by Italian Research Ministry (MIUR) grants COFIN2000 (MM02037133) and COFIN2003 (No. 2003020150).

References

Barrow, J. D., Bhavsar, S. P., & Sonoda, D. H. 1984, MNRAS, 210, 19P
Bernardeau, F., Colombi, S., Gaztañaga, E., & Scoccimarro, R. 2002, Phys. Rep., 367, 1
Bertin, E., & Arnouts, S. 1996, A&AS, 117, 393
Blaizot, J., Guiderdoni, B., Devriendt, J. E. G., et al. 2004, MNRAS, 352, 571
Blaizot, J., Wadadekar, Y., Guiderdoni B., et al. 2005, MNRAS, 360, 159
Bottini, D., Garilli, B., Maccagni, D., et al. 2005, A&A, submitted [arXiv:astro-ph/0409252]
Eke, V. R., Cole, S., & Frenk, C. S. 1996, MNRAS, 282, 263
Fisher, K. B., Davis, M., Strauss, M. A., Yahil, A., & Huchra, J.P. 1994, MNRAS, 267, 927
Giacconi, R., Zirm, A., Wang, J., et al. 2002, ApJS, 139, 369
Guzzo, L., Strauss, M. A., Fisher, K. B., Giovanelli, R., & Haynes, M. P. 1997, ApJ, 489, 37
Hamilton, A. J. S. 1993, ApJ, 417, 19
Hatton, S., Devriendt, J. E. G., Ninin, S., et al. 2003, MNRAS, 343, 75
Hawkins, E., Maddox, S., Cole, S., et al. 2003, MNRAS, 346, 78
Hernquist, L. 1990, ApJ, 356, 359
Kaiser, N. 1986, MNRAS, 219, 785
Kaiser, N. 1987, MNRAS, 227, 1
Landy, S. D., & Szalay, A. S. 1993, ApJ, 412, 64
Le Fèvre, O., Vettolani, G., Maccagni, D., et al. 2003, The Messenger, 111, 18
Le Fèvre, O., Mellier, Y., McCracken, H. J., et al. 2004, A&A, 417, 839
Le Fèvre, O., Vettolani, G., Garilli, B., et al. 2005a, A&A, 439, 845
Le Fèvre, O., Guzzo, L., Meneux, B., et al. 2005b, A&A, 439, 877
Maddox, S. J., Efstathiou, G. Sutherland, W. J., & Loveday, J. 1990, MNRAS, 242, 43P
McCracken, H. J., Radovich, M., Bertin, E., et al. 2003, A&A, 410, 17
Peebles, P. J. E. 1973, ApJ, 185, 413
Peebles, P. J. E. 1980, The Large Scale Structure of the Universe (Princeton: Princeton University Press)
Press, W. H., Teukolsky, S. A., Vetterling, W. T., & Flannery, B. P. 1992, Numerical Recipes in fortran 77: The Art of Scientific Computing, Second Edition (Cambridge: Cambridge University Press)
Robin, A. C., Reylé, C., Derrière, S., & Picaud, S. 2003, A&A, 409, 523